ZIBELINE INTERNATIONAL PUBLISHING

ISSN: 2616-5961 (Online)
CODEN: IMCSBZ

Information Management and Computer Science (IMCS)

DOI: http://doi.org/10.26480/imcs.01.2026.01.11

REVIEW ARTICLE

ADAPTIVE AND ROBUST CONTROL FOR UNCERTAINTY MANAGEMENT IN AUTONOMOUS VEHICLES : THE CASE OF SEGWAY

Arold's Elian Kankeu Kenne[a,b,*], Pascal Kameni[a,b,c], Ibrar Ahmad[d], Maxim Idriss Meli Tametang[e], David Yemele[e]

[a]Department of Mechanical Engineering, Faculty of Engineering, University of Sherbrooke, Sherbrooke, QC J1K 2R1, Canada.
[b]Interdisciplinary Institute for Technological Innovation(3IT), Sherbrooke, QC J1K 0A5, Canada
[c]Center for Research on Aging, Sherbrooke, QC J1H2J7, Canada
[d]College of Biosystems Engineering and Food Science, Zhejiang University, Hangzhou 310058, China
[e]Department of Physics, Faculty of Science, Research Unit for Mechanics and Modeling of Physical Systems, University of Dschang, Dschang, P.O. Box69, Cameroon
**Corresponding author email: Arold's.Elian.Kankeu.Kenne@USherbrooke.ca*

This is an open access article distributed under the Creative Commons Attribution License, which permits unrestricted use, distribution, and reproduction in any medium, provided the original work is properly cited.

ARTICLE DETAILS

Article History:

Received 23 October 2025
Revised 18 November 2025
Accepted 01 December 2025
Available online 02 January 2026

ABSTRACT

In recent years, Segway robots have emerged as a promising solution for urban mobility, thanks to their maneuverability and energy efficiency. However, their nonlinear and unstable dynamics require adapted control strategies. This article presents a complete modeling of the system using the Lagrangian formalism, followed by linearization around equilibrium. Classical control approaches, notably PID controllers, although commonly used, show limited performance in terms of trajectory tracking. To overcome these limitations, a state feedback LQR controller has been synthesized for improved trajectory tracking. To overcome the inaccessibility of internal states, a Kalman observer was designed for the first time ever for this type of system. An adaptive controller of the MRAC type was synthesized to manage user mass uncertainties. Based on a frequency analysis, the simulation results confirm the robustness of the synthesized controller. This opens up promising prospects for the design of self-balancing mobility systems.

KEYWORDS

Segway, Nonlinear Dynamics, Optimal Control, Kalman Observer, MRAC, Robustness

1. INTRODUCTION

Faced with ever-increasing oil consumption and the gradual depletion of fossil fuels, the need to design more energy efficient and environmentally friendly means of transport has become a major challenge. Against this backdrop, electric vehicles are attracting growing interest, particularly in the manufacturing sector, where requirements in terms of performance, autonomy and on-board intelligence are constantly increasing (Chantarachit.S et al.,2019). Among these emerging solutions, the Segway vehicle stands out as an innovative, all-electric, zero-emission personal transporter, distinguished by its exceptional maneuverability and ability to maintain balance thanks to an intelligent stabilization system. Developed by Dean Kalmen and patented in 2001, the segway relies on a sophisticated device combining motors, gyroscopes, on-board computers and reactive actuators to ensure dynamic balance in real time (Chantarachit, et al., 2019). It has been proposed as a means of personal transport because of its great manoeuvrability and small size (Choi et al., 2008; Yin et al., 2007; Grasser et al., 2002; Morrell et al., 2007).

Its operation, based on the permanent adjustment of wheel rotation speeds in response to the user movements, is similar to the principle of the inverted pendulum mounted on wheels, a physical structure known for its natural instability and its interest in control robotics. The robot continuously detects variations in tilt angle and their time derivative, enabling the controller to instantly compensate for any potential imbalance (Navinkumar et al., 2022). The device sensors must continuously measure the state of the machine and transmit this information to the computer controller (Iwashita, et al.,2021). The latter then uses this feedback signal to adjust the wheel speed so that the forward/reverse (pitching) motion is kept within an acceptable range, thus preventing the machine and rider from falling off (Sharma et al., 2015). This behavior has motivated a vast scientific literature focused on the modeling and control of unstable systems. Several previous works have explored various control approaches to improve the robustness and accuracy of the Segway under varying operating conditions. These range from classical PID methods to optimal controllers, including the integration of advanced sensors, obstacle avoidance algorithms and data fusion filters.

In 2012, a group research proposed a framework for dynamic navigation of an autonomous personal transporter, capable of tracking moving targets while avoiding obstacles (Todaka et al., 2012). Their approach integrates localization and avoidance algorithms for adaptive urban mobility. A year later, developed a robotic platform for autonomous maneuvering of a Segway, modeled as an unstable inverted pendulum (Wong, 2013). Using an approach combining dynamic modeling, servomotor control and sensors (infrared, ultrasound, camera), they designed a system capable of automatically stabilizing and steering the vehicle. In 2016, designed a self-balancing prototype using a complementary filter (accelerometer/gyroscope) on platform, with C++ control (Babazadeh et al., 2016). Their system demonstrates the feasibility of a 0° inverted pendulum stabilizer.

A study designed a low-cost Segway stabilized by gyroscope/accelerometer, managing 80 kg over several km (Hespanha., 2007). In 2015, develop an optimal controller for an electric Segway,

Quick Response Code	Access this article online	
	Website: www.theimcs.org	DOI: 10.26480/imcs.01.2026.01.11

Cite the Article: Arold's Elian Kankeu Kenne, Pascal Kameni, Ibrar Ahmad, Maxim Idriss Meli Tametang, David Yemele (2026). Adaptive and Robust Control For Uncertainty Management in Autonomous Vehicles : The Case Of The Segway. Information Management and Computer Science, 9(1): 01-11.

aiming to solve two major challenges: battery energy management and stabilization of its complex nonlinear dynamics. Simulations demonstrated the superiority of this method, particularly in adapting to varying dynamic constraints (Hespanha., 2007). A little later, develops a robust control strategy for a Segway, using a modified LQR controller adapted to load variations (Babazadeh et al., 2016). Their approach combines dynamic modeling using the Newton-Euler method with linearization around the equilibrium point, enabling the vehicle to be stabilized despite non linearities and uncertainties linked to the driver weight..

In line with this approach, this paper proposes the development of an optimal and robust controller for a Segway vehicle, integrating both the management of parametric uncertainties and resistance to external disturbances. This contribution aims to enrich the existing literature by providing a rigorous controller design methodology, as well as a theoretical basis applicable to advanced self-balancing vehicle control.

The remainder of this paper is structured as follows:

Section 2 presents the non-linear dynamics of the Segway, combining the motion of the user and that of the cart, established using the Lagrange formalism. Section 3 focuses first on determining the state representation of the Segway by linear approximation, and then on the stability analysis of the open-loop system. Section 4 focuses on testing the controllability and observability of the system, followed by the design of an optimal state feedback and output feedback controller. Section 5 looks at adaptive control, Section 6 at robust control. Finally, Section 7 provides concluding remarks, summarizing the key findings and contributions of this research.

2. System Modeling

Figure 1: Situation of a segway vehicle in motion

Figure 1, illustrates a real-life situation involving a user on a Segway type personal transporter and all the possible maneuvers the robot can perform. Case a show a backward maneuver, case b shows no maneuver and case c shows a forward maneuver. This is the basis for the equivalent mechanical system of our personal transporter shown in Figure 2.

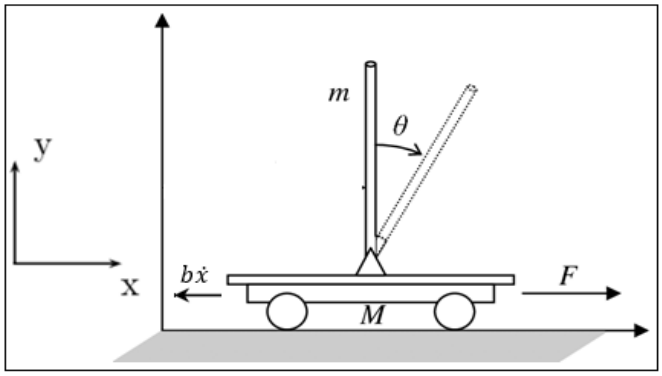

Figure 2: Dynamic model of the two-wheeled inverted pendulum transporter

Figure 2, shows a simplified physical model of the real Segway personal transporter system, represented by an inverted pendulum mounted on a cart. In this diagram, the user is assimilated to a rigid rod of mass m and length l, characterized by a moment of inertia I around its center of mass. The mobile support, consisting of the platform and the motor, is assimilated to a cart of mass M. A driving force F, proportional to the torque generated by the motor and the control signal u, acts horizontally on the cart. Viscous friction, characterized by a coefficient b, models the mechanical losses associated with displacement. The magnitudes x and θ refer respectively to the horizontal position of the carriage and the inclination range of the rod.

Table 1: Main parameters and their values of a Segway

Parameters	Values
Segway Mass, M	10 kg
User Mass, m	100 kg
Coefficient of friction for cart, b	0.25
length to the user center of mass, l	1.7 m
User mass moment of inertia, I	2.5 Kg. m^2
Gravitational acceleration, g	9.8 m/s^2

2.1 Lagrangian Theory

Figure 1, illustrates the Segway vehicle studied in this article, while Fig. 2, offers an equivalent physical representation in the form of an inverted pendulum mounted on a carriage. From this mechanical model, the equation of motion governing the dynamics system is established by applying Lagrange formalism, allowing for interactions between kinetic and potential energies, as well as generalized forces acting on the system as a whole.

The total kinetic energy of the system is calculated according to Eq. (1):

$$T = \frac{1}{2}M\dot{x}^2 + \frac{1}{2}m\left(\dot{x}^2 + 2l\dot{x}\dot{\theta}\cos\theta + l^2\dot{\theta}^2\right) + \frac{1}{2}I\dot{\theta}^2 \quad (1)$$

As the carriage is moving on a horizontal rail, only the moving pendulum has potential energy. In the same way, we calculate the potential energy of the pendulum center of gravity according to Eq. (2):

$$U = mgl\cos\theta \quad (2)$$

The Lagrangian of the system is obtained from the two energies and is calculated in Eq. (3):

$$L = \frac{1}{2}M\dot{x}^2 + \frac{1}{2}m\left(\dot{x}^2 + 2l\dot{x}\dot{\theta}\cos\theta + l^2\dot{\theta}^2\right) + \frac{1}{2}I\dot{\theta}^2 - mgl\cos\theta \quad (3)$$

The general equation of motion based on Lagrange theory is given by Eq. (4):

$$\frac{d}{dt}\left(\frac{\partial L}{\partial \dot{q}_i}\right) - \frac{\partial L}{\partial q_i} = -\frac{\partial F_d}{\partial \dot{q}_i} + F_i \quad (4)$$

with $j = (1,2) = (x, \theta)$

Where q_i is the generalized coordinate of the system, $\dot{q}_i$ the generalized velocity, F_i the generalized force associated with q_i and F_d the dissipative force given by the equation below in Eq. (5):

$$F_d = -b\dot{x} \quad (5)$$

2.2 Dynamic Model

By combining the two previously established mechanical models, we obtain a global dynamic, presented by Eq. (6), in which the input corresponds to the voltage applied to the DC motor and the output represents the physical position of the Segway. This integrated model forms the basis of the controller synthesis developed in the remainder of this article.

The projection of Eq (4) for each value of j, gives us the dynamics of the system:

$$\begin{cases}(M+m)\ddot{x}+b\dot{x}+ml\cos(\theta)\ddot{\theta}-ml\sin(\theta)\dot{\theta}^2=F\\ (I+ml^2)\ddot{\theta}+ml\cos\theta\ddot{x}+mgl\sin\theta=0\end{cases} \quad (6)$$

This equation can be reformulated as a Cauchy problem, so that numerical solutions can be found using suitable numerical integration methods.

3. Analytical Segway Model

3.1 Linear model in State-Space Form

The nonlinear Segway equation is linearized by a Taylor series approximation around the equilibrium point $\theta = 0$ as follows: From the Taylor series expansion, the approximation of any function of θ is expressed in Eq. (7):

$$f(\theta) \approx f(\theta_0) + \varepsilon \left.\frac{df}{d\theta}\right|_{\theta_0} \quad (7)$$

From this Eq. (7), we can introduce a new variable φ which is expressed in Eq. (8):

$$\theta = \pi + \Phi \quad (8)$$

Taking into account this change of variable, we have the following transformations represented in Eq. (9):

$$\begin{cases}\cos\theta = \cos(\pi+\Phi) = -1\\ \sin\theta = \sin(\pi+\Phi) = -\varphi\end{cases} \quad (9)$$

Considering the system of Eq. (9), we obtain the following equality: $\dot{\theta}^2 = \dot{\Phi}^2 = 0$

The linearized model of the Segway, expressed in Eq. (10), is derived as follows:

$$\begin{cases}\dot{x} = f(x,u)\\ y = h(x,u)\end{cases} \quad (10)$$

Where f and h are smooth applications; $x \in \mathbb{R}^n$ and $u \in \mathbb{R}^p$.

Eq. (9) can be rewritten with the matrices A, B, C and D as shown in Eq. (11).

$$\begin{cases}\frac{dx}{dt} = Ax + Bu\\ y = Cx + Du\end{cases} \quad (11)$$

By denoting the system state vector by $x = \left[x\ \dot{x}\ \theta\ \dot{\theta}\right]^T$, the dynamics system can be formulated within the framework of the state representation, which consists of two equations: an evolution equation describing the internal dynamics of the system, and an output equation linking the measured variables to the state.

The system under consideration typically belongs to the class of multivariable systems shown in Eqs. (12) and (13), where the input u corresponds to the voltage applied to the motor, while the outputs x and Φ designate the position of the cart and the angle of inclination of the pendulum respectively.

Evolution equation:

$$\begin{bmatrix}\dot{x}\\ \ddot{x}\\ \dot{\Phi}\\ \ddot{\Phi}\end{bmatrix} = \begin{bmatrix}0 & \frac{1}{(I+ml^2)b} & \frac{0}{m^2gl^2} & \frac{0}{0}\\ 0 & -\frac{}{I(M+m)+Mml^2} & \frac{}{I(M+m)+Mml^2} & 0\\ 0 & \frac{0}{mlb} & \frac{0}{mgl(M+m)} & 1\\ 0 & -\frac{}{I(M+m)+Mml^2} & \frac{}{I(M+m)+Mml^2} & 0\end{bmatrix}\begin{bmatrix}x\\ \dot{x}\\ \Phi\\ \dot{\Phi}\end{bmatrix} + \begin{bmatrix}0\\ \frac{(I+ml^2)}{I(M+m)+Mml^2}\\ 0\\ \frac{ml}{I(M+m)+Mml^2}\end{bmatrix} u \quad (12)$$

Output equation:

$$y = \begin{bmatrix}1 & 0 & 0 & 0\\ 0 & 0 & 1 & 0\end{bmatrix}\begin{bmatrix}x\\ \dot{x}\\ \Phi\\ \dot{\Phi}\end{bmatrix} + \begin{bmatrix}0\\ 0\end{bmatrix} u \quad (13)$$

3.2 Segway stability analysis in open loop

The aim of this subsection is to determine the equilibrium points of the system in the absence of external control, i.e. for $u = 0$, corresponding to a natural equilibrium. Eq. (14) presented an equilibrium point is defined as a state x_e for which the system dynamics remain stationary. These states are obtained by solving the equation $Ax_e = [0]_{,,}$ where A denotes the dynamics matrix of the linearized system.

$$\underbrace{\begin{bmatrix}0 & \frac{1}{(I+ml^2)b} & \frac{0}{m^2gl^2} & 0\\ 0 & -\frac{}{I(M+m)+Mml^2} & \frac{}{I(M+m)+Mml^2} & 0\\ 0 & \frac{0}{mlb} & \frac{0}{mgl(M+m)} & 1\\ 0 & -\frac{}{I(M+m)+Mml^2} & \frac{}{I(M+m)+Mml^2} & 0\end{bmatrix}}\begin{bmatrix}x_e\\ \dot{x}_e\\ \Phi_e\\ \dot{\Phi}_e\end{bmatrix} = \begin{bmatrix}0\\ 0\\ 0\\ 0\end{bmatrix} \quad (14)$$

Solving this system of equations yields two possible equilibrium solutions which are expressed in Eq. (15):

$$\begin{cases}\mathbf{x_{e1}} = (\mathbf{x_e}, \mathbf{0}, \mathbf{0}, \mathbf{0})^T\\ \mathbf{x_{e2}} = (\mathbf{x_e}, \mathbf{0}, \boldsymbol{\pi}, \mathbf{0})^T\end{cases} \quad (15)$$

The two configurations mentioned correspond respectively to the equilibrium regimes of the inverted pendulum and the simple pendulum. In this study, centered on the control of a Segway type robot, representing an emblematic application of the inverted pendulum, the analysis will be conducted from the unstable equilibrium associated with the $\mathbf{x_{e1}}$ equilibrium point. This choice is motivated by the need to guarantee stabilization around the unstable vertical position typical of self balancing systems. This section presents the open-loop analysis of the Segway system using MATLAB Simulink dynamic modeling, based on the implementation of the system's differential equations as block diagrams as described in Figure 3. Impulse excitation is applied to the input in order to observe the temporal response and assess the system natural stability, with a view to subsequent synthesis of a closed loop control. MATLAB Simulink environment was used to simulate and visualize the dynamic system behavior. Figure 4 and Figure 5, illustrate the evolution of the carriage longitudinal position and the pendulum displacement, respectively.

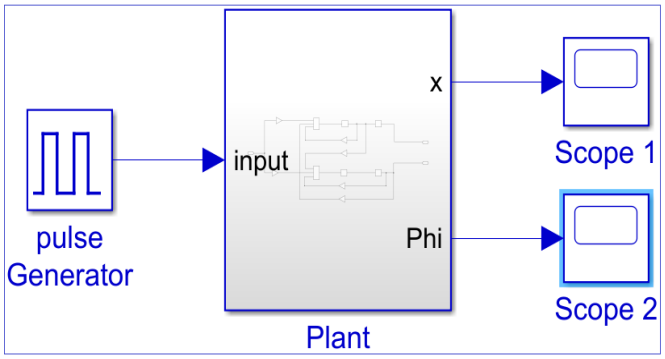

Figure 3: Simulink model of the Segway with impulse excitation

Scope 1 shows the displacement of the cart, while Scope 2 shows the oscillation of the pendulum, facilitating rigorous analysis of the system response to the pulse excitation applied to the input, and the development of control laws.

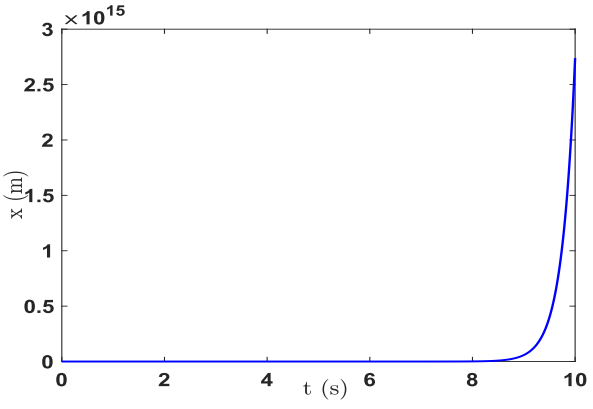

Figure 4: Time evolution of the longitudinal position of the cart in response to a pulse type excitation

Fig. 4, illustrates the time trajectory of the carriage representing Segway moving platform. Although the equilibrium point at position $\mathbf{x_e}$ could

theoretically take on an arbitrary value, the simulation shows an unbounded exponential drift, incompatible with realistic physical operation. This divergence reflects the lack of stabilization of the horizontal dynamics, which could compromise the integrity of the system.

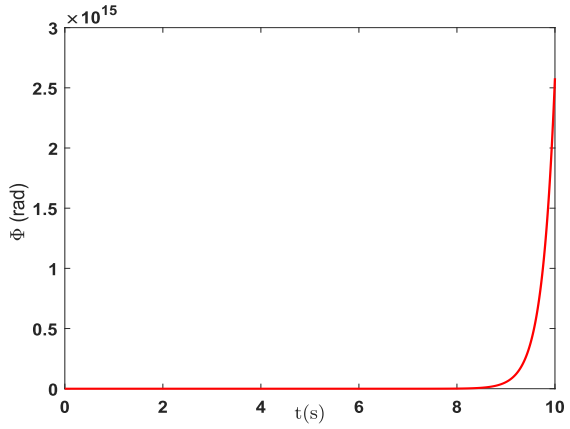

Figure 5: Time evolution of the pendulum angle of inclination in response to an impulse load

Fig. 5, shows the temporal evolution of the angle of inclination of the rod, expressed in radians. An exponential increase in this angle is observed from 9 s onwards, reflecting a rapid loss of system equilibrium. This divergent behavior highlights the intrinsic instability of the inverted pendulum in the absence of regulation. As such dynamics are incompatible with the stability requirements of a real physical system, the implementation of a controller is essential.

4. Control Theory

In control theory, the main objective is to control the state or output of a dynamic system to follow a reference trajectory, based on a control law developed from real-time measurements. The choice of control strategy directly determines the nature and effectiveness of the corrective actions applied. Among existing approaches, optimal control is particularly relevant to the stabilization of complex dynamic systems such as the Segway. The model studied integrates four state variables: the longitudinal position of the carriage, the angle of inclination with respect to the vertical, and their associated speeds, all accessible via on-board measurement devices.

4.1 Testing of system controllability and observability

A time-invariant linear system is said to be completely controllable if and only if its controllability matrix:

$$C = [B \ A^2B \dots \ A^{n-1}B] \tag{16}$$

is of maximum rank, i.e. equal to n, the dimension of the state space. This property guarantees that it is possible, starting from any initial condition, to move the state of the system to any other position in the state space via an appropriate command.

$$C_0 = \begin{bmatrix} 0 & 0.0324 & -0.0002 & 0.2926 \\ 0.0324 & -0.0002 & 0.2926 & -0.0042 \\ 0 & 0.0187 & -0.0001 & 0.2754 \\ 0.0187 & -0.0001 & 0.2754 & -0.0032 \end{bmatrix} \tag{17}$$

Calculation of the rank of the controllability matrix C_0, using the MATLAB function rankC_0, verifies the system controllability property. Obtaining a rank equal to 4, corresponding to the dimension of the state space, confirms that the dynamic model of the Segway studied is fully controllable.

Analogously, a linear system is said to be fully observable if the observability matrix

$$O = \begin{bmatrix} C \\ CA \\ CA^2 \\ \vdots \\ CA^{n-1} \end{bmatrix} \tag{18}$$

is of rank n, where n denotes the dimension of the state space. This property guarantees that it is possible to reconstruct the state of the system from the input and output signal.

$$Ob = \begin{bmatrix} 1 & 0 & 0 & 0 \\ 0 & 0 & 1 & 0 \\ 0 & 1 & 0 & 0 \\ 0 & 0 & 0 & 1 \\ 0 & -0.0071 & 15.6130 & 0 \\ 0 & -0.0041 & 14.6946 & 0 \\ 0 & 0.0001 & -0.1113 & 15.6130 \\ 0 & 0 & -0.0644 & 14.6946 \end{bmatrix} \tag{19}$$

Rank 4 of this observability matrix is calculated using the Matlab rankOb function. This confirms the complete observability of the segway modeled in this article.

4.2 Optimal Control: Control by state feedback.

Among advanced control techniques in automation, optimal control is distinguished by the optimization of a cost criterion, usually quadratic, as a function of states and commands. The control diagram used for the remainder of this article is shown in Figure 6 below.

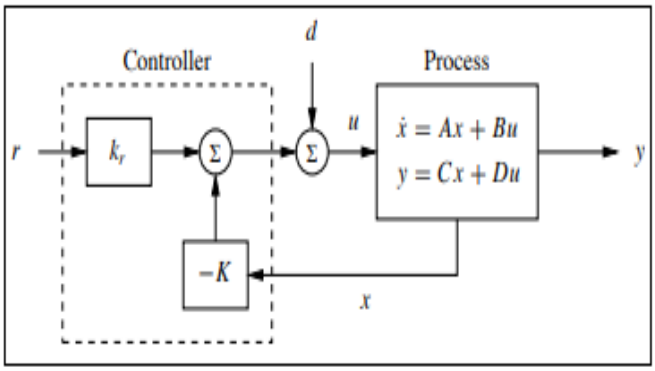

Figure 6: Block diagram of a control system with state feedback. The controller uses the system state x and the reference input r to control the process via its input u. We model disturbances via the additive input u.

Consider a linear multi-input system described by Eq. (20):

$$\begin{cases} \frac{dx}{dt} = Ax + Bu \\ y = Cx + Du \end{cases} \quad x \in \mathbb{R}^n, u \in \mathbb{R}^p \tag{20}$$

The objective of linear quadratic optimal control (LQR) is to determine a control law u(t) that minimizes the quadratic cost function presented in Eq. (21) as follows:

$$J_{LQR} = \int_0^\infty (x^T Q_x x + u^T Q_u u)dt \tag{21}$$

Where $Q_x \geq 0$ and $Q_u \geq 0$ are symmetrical positive semidefinite matrices, respectively weighting states and control efforts. This cost function reflects a compromise between minimizing the deviation of the state from the origin and the energy consumption associated with control. By adjusting Q_x and Q_u, it is possible to regulate the convergence speed of the system while limiting the amplitude of the control action. The optimal solution to the LQR problem is given by a linear state feedback law deduced from Eq. (22) as follows:

$$u = -Q_u^{-1}B^T P x \tag{22}$$

Where $P \in \mathbb{R}^{n*n}$ is a symmetrical positive definite matrix that satisfies the equation:

$$PA + A^T P - PBQ_u^{-1}B^T P + Q_x = 0 \tag{23}$$

The main difficulty lies in the judicious choice of the weighting matrices Q_x and Q_u. A common approach is to adopt the diagonal matrices shown in Eqs. (24) and 25 to simplify their parameterization.

$$Q_x = \begin{bmatrix} q_1 & \cdots & 0 \\ \vdots & \ddots & \vdots \\ 0 & \cdots & q_n \end{bmatrix} \tag{24}$$

and

$$Q_u = \begin{bmatrix} \rho_1 & \cdots & 0 \\ \vdots & \ddots & \vdots \\ 0 & \cdots & \rho_n \end{bmatrix} \quad (25)$$

The optimal feedback gain K obtained by solving the Riccati equation is deduced from Eq. (26) as follows:

$$K = [K_x \quad K_{\dot{x}} \quad K_\Phi \quad K_{\dot{\Phi}}] \quad (26)$$

In this gain vector, K_x corresponds to the control gain associated with the Segway position, $K_{\dot{x}}$ corresponds to the velocity control gain of the Segway body, K_Φ is the gain related to the pendulum angular position, and $K_{\dot{\Phi}}$ represents the gain for the pendulum angular velocity. Each component is crucial for stabilizing the system and ensuring the desired dynamic response of the Segway.

In this work, we strongly penalize the system output in order to have a fast and stable response. The Figure 7 above shows the closed-loop state feedback control architecture implemented in the Simulink environment for the control of the Segway system. The control signal is injected into the dynamic model, and outputs such as carriage position and pendulum angle.

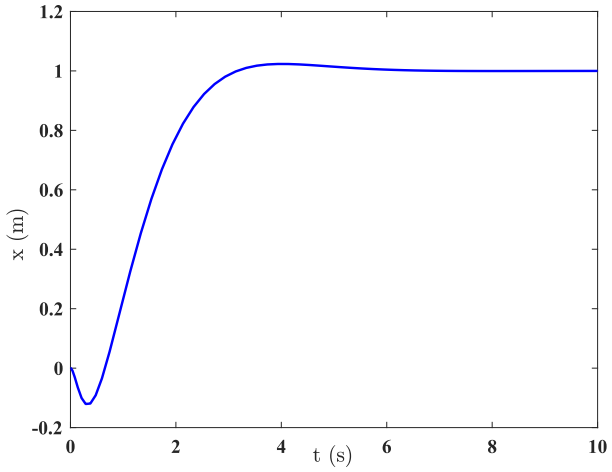

Figure 7: Cart stabilization by feedback with optimal control

Figure 7, shows the time response of the carriage position under feedback control. This converges to a finite value close to 1m, with a slight initial overshoot followed by a rapidly damped transient regime. This behavior highlights the performance of the optimal controller designed, ensuring effective stabilization of the system. Unlike the open-loop configuration, where the position diverged continuously, the implemented control prevents any drifting of the carriage and guarantees a controlled dynamic response.

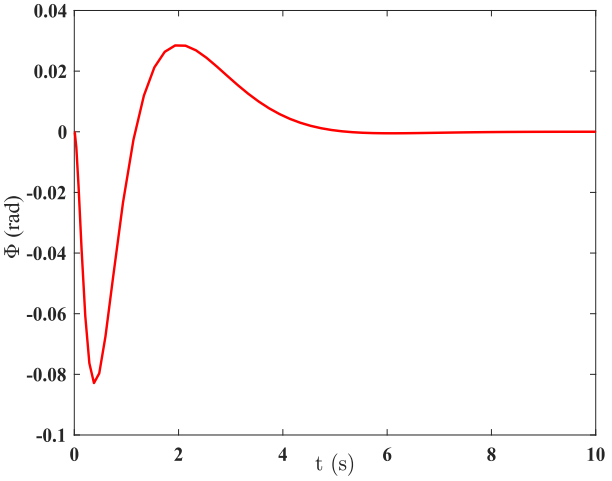

Figure 8: Pendulum stabilization by state feedback with optimal control

Figure 8, shows the temporal response of the pendulum, demonstrating stabilization of the angle of inclination at around 0 radian. Transient oscillations are rapidly damped, indicating convergence to vertical equilibrium in a short time. This performance testifies to the effectiveness of the optimal controller implemented, capable of compensating for inertial effects and external disturbances to keep the pendulum vertical.

4.3 Kalman state observer

This section deals with the implementation of a state observer to estimate the system internal variables from inputs and output measurements, for effective feedback. Since observability analysis has shown that the system is fully observable, reconstruction of internal states is theoretically feasible. Unlike state feedback control, which relies on the often-unrealistic assumption of direct access to all states, the use of an observer enables values to be deduced from a dynamic model, exploiting only measurable input and output information.

4.3.1 Definition of Observability

Consider the following system of Eq. (27):

$$\frac{dx}{dt} = Ax + Bu, y = Cx + Du \quad (27)$$

Where $x \in \mathbb{R}^n$ is the state, $u \in \mathbb{R}^p$ the input and $y \in \mathbb{R}^q$ the measured output.

A linear system is said to be observable when it is possible, from measurements of the input u(t) and the output y(t) over a finite time interval [0, T], to fully reconstruct the internal state x(T). Observability implies that no dynamic component of the system escapes detection via the measured signals, thus ensuring complete knowledge of its behavior. This is of fundamental importance in practice, particularly when it comes to assessing the suitability of the sensors available for implementing an effective control strategy. The state observer control scheme used in the remainder of this article is shown in Figure 9 as follows.

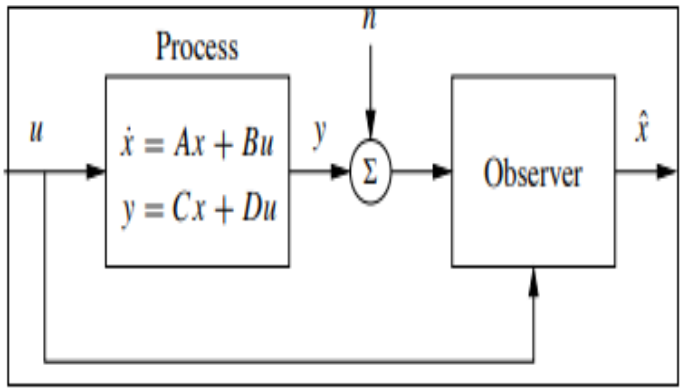

Figure 9: Block diagram of an observer. The observer uses the process measurement y (often altered by noise n) and the input u to estimate the current state of the process, denoted $\hat{x}$.

4.3.2 State estimator

Once the observability of the system has been verified, it is possible to design a state observer capable of estimating the internal variables from the input and output signals. The objective is then to construct an auxiliary dynamic system whose form is deduced from the Eq. (28) as follows:

$$\frac{d\hat{x}}{dt} = F\hat{x} + Gu + Hy \quad (28)$$

where $\hat{x} \in \mathbb{R}^n$is an estimate of the actual state x with $\hat{x}(t) \to x(t)$ when $t \to \infty$. Considering the state system with no direct term($D = 0$) according to Eq. (29) below:

$$\dot{x} = Ax + Bu, y = Cx + [0]u \quad (29)$$

A naive estimator based solely on the dynamics of the system is deduced from Eq. (30) as follows:

$$\dot{\hat{x}} = A\hat{x} + Bu \quad (30)$$

The estimation error $\tilde{x} = x - \hat{x}$, evolves according to the following Eq. (31):

$$\frac{d\tilde{x}}{dt} = A\tilde{x} \quad (31)$$

If the eigenvalues of A are in the left half-plane, the estimated state $\hat{x}$

converges slowly to zero. On the other hand, if A is unstable, the estimate will diverge. To overcome these limitations, a corrective term proportional to the error between the measured and estimated output is introduced into the observer structure**.** This can be seen in the following Eq. (32):

$$\begin{cases} \dfrac{d\hat{x}}{dt} = A\hat{x} + Bu + L(y - \hat{y}) \\ \hat{y} = C\hat{x} + [0]u \end{cases} \quad (32)$$

The gain L, calculated using the Matlab function lqe, is adjusted to accelerate convergence. Unlike the simple estimator, the observer actively corrects its estimate in real time, ensuring fast and robust state reconstruction, even for an unstable system.

The Simulink diagram shown in Figure 9, illustrates the implementation of a state observer connected to a plant. The pulse generator provides the input common to both blocks, while the observer uses the output measurements of the real system to reconstruct the estimated internal states $\hat{x}$ and $\hat{y}$. A probe placed at the output allows us to visualize the temporal evolution of the estimated outputs and compare them to the real outputs, respectively, which facilitates the evaluation of the observer accuracy.

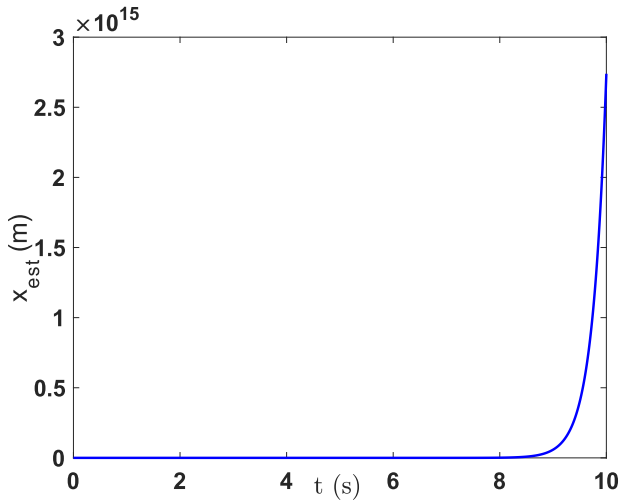

Figure 10: Estimating the linear position of the cart

The output shown in Figure 10, corresponds to the reconstruction of the carriage position from the state observer. It can be seen that the estimated trajectory perfectly follows the actual position obtained previously, without any significant deviation or offset. This superposition of curves validates the accuracy of the designed observer and demonstrates its ability to faithfully estimate the dynamic evolution of the carriage based solely on output measurements and known inputs. The output displayed in Figure 11, represents the estimated position of the pendulum, calculated by the state observer. There is remarkable agreement between the estimated trajectory and that actually measured, reflecting the model stability to faithfully reproduce the pendulum dynamics, despite its instability.

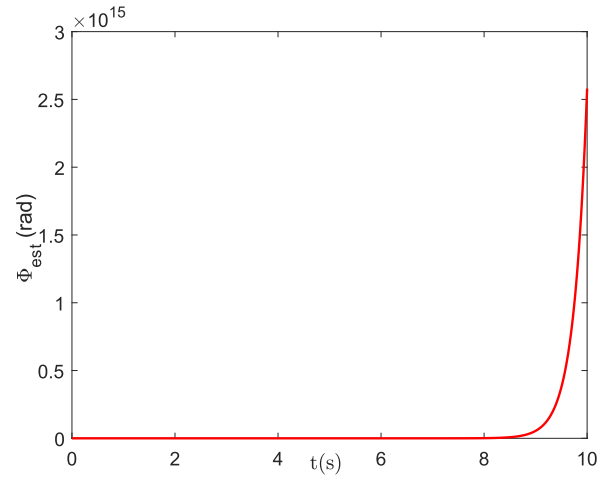

Figure 11: Estimating the angular position of the pendulum

This precision in the reconstruction of the angular state highlights the effectiveness of the observation scheme implemented.

4.4 Control Using Estimated State

In this section, we take up the system defined in Eq. (32).The aim is to design a state feedback control law when only the output is measured. As established in section (4.1), the system is both controllable and observable. An observer was developed in section (4.3), to estimate states $\hat{x}$ from inputs and outputs. As not all states are measurable, we propose a state estimation control in the form of Eq. (33) below:

$$u = -K_x\hat{x} + k_r r \quad (33)$$

The diagram shown in Figure 12 illustrates the complete architecture of the control system, including the state estimator. This device reconstructs the internal variables from the available inputs and outputs and then applies a control law. The aim is to ensure precise tracking of the cart reference position while maintaining the pendulum equilibrium. This architecture integrates MATLAB Simulink modules. The previously designed observer, together with the synthesized optimal controller, enables efficient closed-loop control.

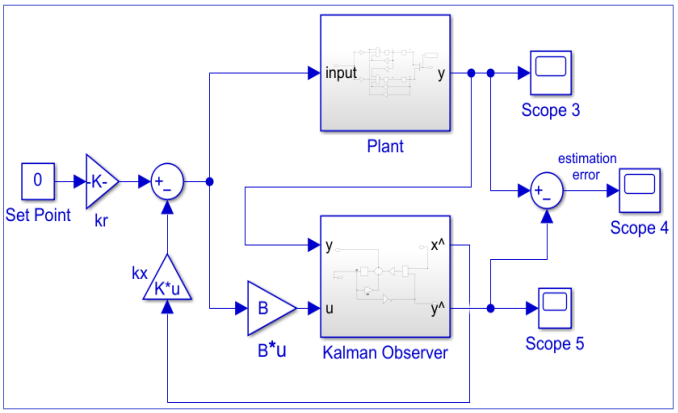

Figure 12: Block diagram of an observer-based control system. The observer uses the measured output y and input u to construct a state estimate. This estimate is used by a state feedback controller to generate the corrective input. The controller consists of the observer and the state feedback.

As part of the control architecture based on state estimation, it is essential to validate the quality of the outputs reconstructed by the observer. The Scope 5 in Figure 12 displays the estimated system output. This visualization provides an assessment of the fidelity of the estimation process in relation to the measured signals and is a key indicator for judging the consistency between the observer internal model and the actual dynamics of the system.

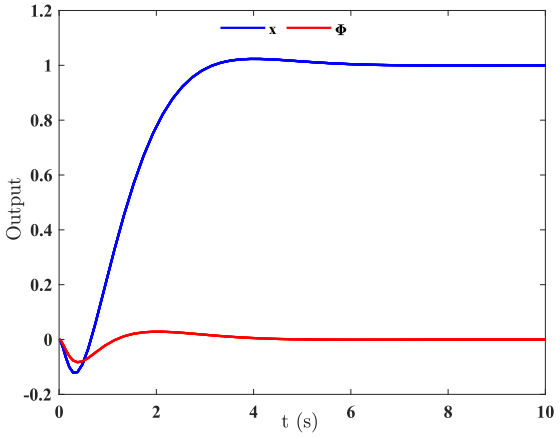

Figure 13: Estimated system output from a state observer

Visualization of the estimated output shows the same pattern as the actual system output. This correspondence confirms the observer stability to reconstruct the dynamics of the output from the estimated internal states with a high degree of accuracy. Such a match indicates that the internal model used in the observer faithfully reflects the behavior of the physical system, thus ensuring the validity of the estimate in the control context. To

quantify the observer performance, scope 6 displays the estimation error, defined as the difference between the actual measured output of the system and the output estimated by the observer. This error characterizes the accuracy of the reconstruction process and is shown in Figure 14.

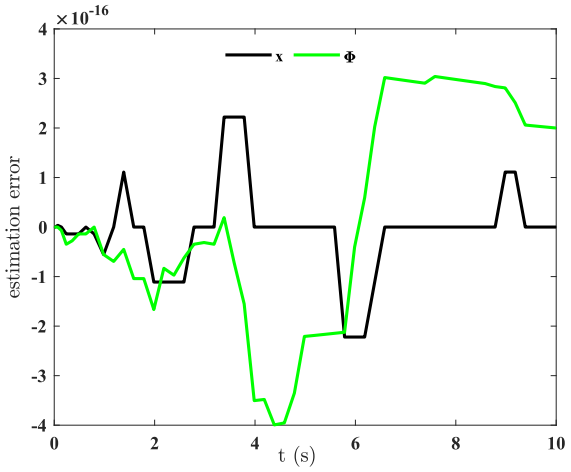

Figure 14: Time evolution of the estimation error

Figure 14 , shows the evolution of the estimation error of the cart position in black and that of the pendulum angle in green. It can be seen that the error is of the order of 10^{-16}, meaning that it is practically zero. It reveals an excellent representation of the real model, attesting to the accuracy of the estimated model. This quality is confirmed by a root mean square error (RMSE ≈ 0) of practically zero, reflecting a very low dispersion between estimated and actual values.

5. ADAPTIVE CONTROL

5.1 General

In the presence of external disturbances or parametric variations, the performance of the nominal controller can degrade significantly, compromising the Segway stability. Adaptive control maintains system performance by adjusting control laws in real time in the face of uncertainties and external disturbances (Ogata, 2010).

The principle of Model Reference Adaptive Control consists in forcing the system to follow the dynamics of an ideal model called reference dynamics, deduced from Eq. (34) as follows (Skogestad, 2005):

$$\begin{cases} \dot{x}_m = A_m x_m(t) + B_m r(t) \\ y(t) = C_m x_m(t) + D_m r(t) \end{cases} \quad (34)$$

Here, $r(t)$ is the external reference signal, and $x_m(t)$ is the state of the reference model. Since $r(t)$ is known, it is possible to simulate the reference model to obtain the trajectory $x_m(t)$.

The matrix A_m is constant and must be Hurwitz, meaning that all its eigenvalues have strictly negative real parts to ensure stability. B_m is the control effectiveness matrix.

This approach enables real-time adjustment of controller parameters to compensate for structural and parametric uncertainties in the system. Initially introduced by Whittaker, then formalized by Yamron, through the MIT rule based on a gradient descent adaptation strategy, it constitutes a systematic method for updating control gains (Pilon, 2019; Landau, 1986). Its aim is to ensure optimum system performance in the presence of dynamic or unknown parameter variations.

A mechanism for parameter adjustment is given by the Lyapunov rule or the MIT rule, expressed according to Eq. (36) as follows (Astrom et al., 2008):

$$\frac{d\theta}{dt} = -\gamma e \frac{\partial e}{\partial \theta} \quad (35)$$

where γ is a parameter, $e = y_m - y$, and $\partial e/\partial\theta$ is a sensitivity derivative.

In this article, we will focus on the Lyapunov rule for determining learning parameters.

5.2 Definition MRAC

5.2.1 Lyapunov Theory

Modern understanding of the stability of nonlinear dynamical systems is largely based on the pioneering work of the russian mathematician A. Lyapunov (Pawar et al., 2015). At the end of 19th century, he was interested in the stability of the origin for an autonomous system whose form is deduced from the following Eq. (36):

$$\dot{x} = f(x) \quad (36)$$

With $f(0) = 0$

In this context, the origin $x(t) = 0$ is a trivial solution. To guarantee the existence and uniqueness of the trajectories, we assume that the function $f(x)$ is locally Lipschitzian in a neighborhood of the origin, i.e. there exists a constant $L > 0$ such that the Eq. (37) is verified:

$$\|f(x) - f(y)\| \leq L\|x - y\| \quad (37)$$

$\forall\, x, y$ close to 0

The Lyapunov method is based on the construction of a continuous, differentiable, positive-definite scalar function $V: \mathbb{R}^n \to \mathbb{R}$, called the Lyapunov function, whose time derivative along the system trajectories satisfies Eq. (38) below:

$$\frac{dV}{dt} = \frac{\partial V^T}{\partial x}\frac{dx}{dt} = \frac{\partial V^T}{\partial x} f(x) = -M(x) \quad (38)$$

If $M(x)$ is positive semidefinite, then the origin is stable in the Lyapunov sense; if $M(x)$ is positive definite, the origin is asymptotically stable. Furthermore, if $V(x) \to \infty$ when $\|x\| \to \infty$ and $\frac{dV}{dt} < 0$ strictly, stability is said to be global and asymptotically stable (Astro et al., 1989).

In the particular case of a linear system satisfying the Eq. (39) below:

$$\dot{x} = Ax \quad (39)$$

If the origin is stable, then for any symmetric positive definite matrix Q, there exists a unique symmetric positive definite matrix P satisfying the algebraic Lyapunov equation deduced from the Eq. (40) as follows:

$$A^T P + PA = -Q \quad (40)$$

The associated quadratic function is presented according to the Eq. 41 as follows:

$$V(x) = x^T P x \quad (41)$$

It is therefore a suitable Lyapunov function for stability analysis, providing a rigorous theoretical framework for assessing the stability of linear and non-linear systems.

5.2.2 MRAC using Lyapunov Theory

The controlled system, which usually has modeling uncertainty and external disturbances, has the nominal equation of state deduced from Eq. 42 as follows:

$$\dot{x}(t) = Ax(t) + B\big(u(t) + f(x)\big) \quad (42)$$

Where $x(t) \in \mathbb{R}^n$ is the system state vector, $u(t) \in \mathbb{R}^p$ is the control input, $A \in \mathbb{R}^{n*n}$, is the state -transition matrix, and $B \in \mathbb{R}^{n*m}$ is the input matrix. The pair (A, B) pair is assumed to be controllable. The function $f(x)$ represents matched uncertainties within the system dynamics. The controller uses this expected nominal plant behavior when updating the controller parameters. The control input $u(t)$ is calculated using both feedback and adaptation components, and is defined according to Eq. 43 as follows:

$$u(t) = k_x x(t) + k_r r(t) - u_{ad} \quad (43)$$

Here, k_x and k_r are the state feedback and feedforward gain matrices, respectively. The term $r(t)$ denotes the external reference signal, while u_{ad} is the adaptive control component that compensates for systems disturbances.

The adaptive control input u_{ad} is modeled according to Eq. (44) as follows:

$$u_{ad} = w^T \varphi(x) \quad (44)$$

Where $\varphi(x)$ contains the features of the disturbance model, and w is an adaptive weight vector associated with these features.

In the case of single hidden layer neural networks, the adaptive control law takes the form of the following Eq. (45):

$$u_{ad} = w^T\sigma(N^Tx) \quad (45)$$

Where N is the weight matrix of the hidden layer, and $\sigma(.)$ is a sigmoid activation function. This formulation allows the controller to approximate nonlinearities in the disturbances using neural networks structures.

The controller computes the error $e(t)$ between the states of the controlled system and the states of the reference model. It then uses that error to adapt the values of kx, kr, and w in real time.

In the MRAC, a reference model is deduced from Eq. (46) as follows:

$$\dot{x}_m(t) = A_m x_m(t) + B_m r(t) \quad (46)$$

Where $A_m \in \mathbb{R}^{n*n}$ is Hurwitz, $x_m(t) \in \mathbb{R}^n$, $B_m \in \mathbb{R}^{n*m}$, and et $r(t) \in \mathbb{R}^m$ denotes a piecewise continuous bounded input and reference signal. A direct linear adaptive control law is proposed according to Eq. (47) below (Narendra, et al., 2012):

$$u(t) = K_x^{d^T}(t)x(t) + K_r^{d^T}(t)r(t) \quad (47)$$

Where $K_x^{d^T} \in \mathbb{R}^{n*m}$and $K_r^{d^T}(t) \in \mathbb{R}^{m*m}$ are real-time adjusted gains.

Injecting (47) into (42), we obtain the following Eq. (48):

$$\dot{x}(t) = \left(A + BK_x^{d^T}\right)x(t) + B\left(K_r^{d^T}r(t) + f(x)\right) \quad (48)$$

For the system to follow the reference model (46), we assume the existence of constant gains K_x and K_r under the assumption of the matching condition below (Tao, 2003):

Assumption: If A and B are known, there are constant matrices $K_x \in \mathbb{R}^{n*m}$ and $K_r \in \mathbb{R}^{m*m}$ such that we have the Eqs. (49) and (50), below:

$$A + BK_x^T = A_m \quad (49)$$

and

$$BK_r^T = B_m \quad (50)$$

Under this assumption, the dynamics of the system is deduced from Eq. (51) as follows:

$$\dot{x} = A_m x + B_m r + B\tilde{K}_x^T x + B\tilde{K}_r^T r \quad (51)$$

with $\tilde{K}_x(t) \triangleq K_x^d(t) - K_x$ and $\tilde{K}_r(t) \triangleq K_r^d(t) - K_r$. The tracking error is deduced from Eq. (52) as follows:

$$e(t) \triangleq x(t) - x_m(t) \quad (52)$$

Combining Eqs. (41), (46) and (47), the error dynamics is deduced from Eq. (53) as follows:

$$\dot{e} = A_m e + B\tilde{K}_x^T x + B\tilde{K}_r^T r \quad (53)$$

The standard direct adaptive updating laws for $K_x^d(t)$ and $K_r^d(t)$ presented by the Eqs. (54) and (55) are given using Lyapunov theory.

$$\dot{K}_x^d = -\Gamma_x x e^T PB \quad (54)$$

$$\dot{K}_r^d = -\Gamma_r r e^T PB \quad (55)$$

Where $\Gamma_x, \Gamma_r > 0$ are positive definite learning matrices, $P \in \mathbb{R}^{n*n}$is the positive definite solution of the Lyapunov equation associated with a positive definite matrix $Q \in \mathbb{R}^{n*n}$.

The equations developed guarantee that the tracking error $e(t) \to 0$ when $t \to \infty$.

Table 2: Control Gains

Gains	Learning rate(Γ_x)	Learning rate (Γ_r)
Values	5.10^3	5.10^3

In order to validate the performance of MRAC, a simulation presented in Figs. 15 and 16 was carried out in MATLAB Simulink on the basis of the adaptation equations deduced using the Lyapunov method. The learning gains Γ_x and Γ_r were carefully selected to enable efficient adaptation of the control gains k_x and k_r in real time. The resulting Simulink diagram shows the evolution of the system in the presence of mass uncertainty. The following figures illustrate the convergence of the controlled output to the reference model output.

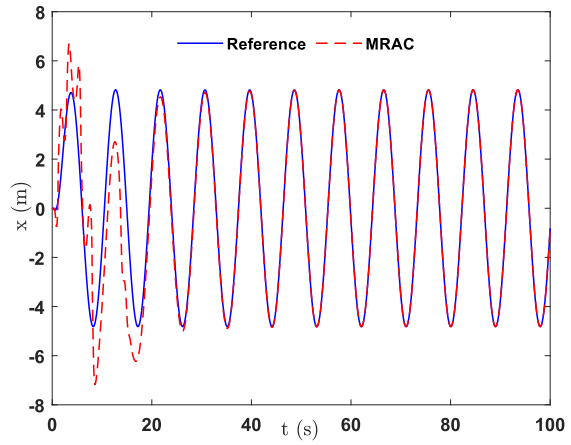

Figure 15: Adaptive MRAC tracking of truck position

Fig. 15 shows the response of the cart position to a sinusoidal reference signal. It can be seen that, initially, the actual output shows greater oscillations than the reference, reflecting an initial poor adaptation of the controller. However, as time progresses, the carriage response becomes increasingly aligned with the reference. This indicates that the MRAC controller is progressively learning online the appropriate gains to match the actual system dynamics to those of the reference model. The carriage then follows the pulses better and better, despite uncertainties in system parameters such as mass, demonstrating the robustness of the adaptation.

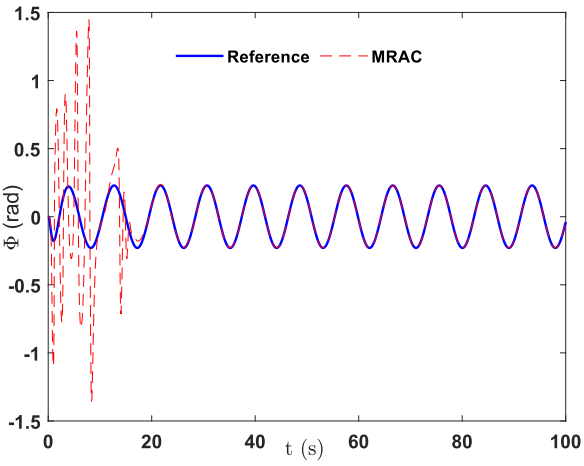

Figure 16: Adaptive MRAC tracking of pendulum angular position

Fig.16 shows the evolution of the pendulum angular position. Initially, the pendulum response (before convergence of the adaptive gains) is shorter, but with strong overshoot, showing that the system is struggling to stabilize the Segway. Over time, however, the pendulum angle converges towards the reference trajectory, revealing improved synchronization and stability. This behavior reflects the effect of MRAC adaptive learning, which adjusts gains to compensate for non-linearities and uncertainties. The system learns to balance the pendulum more and more accurately, aligning its dynamics with those of the imposed model, despite significant initial disturbances.

6. Parametric Robustness

6.1 Frequency analysis

In automation, the robustness of a system refers to its ability to maintain acceptable performance in the presence of parametric uncertainties or

external disturbances (Johan et al., 2021). Frequency analysis, based on transfer function representation, is an essential tool for quantifying this robustness and assessing the stability of a closed-loop system. Calculating the transfer function G(s) with state feedback is crucial for the Bode diagram, which gives the gain $|G(j\omega)|$ and phase $\mathrm{Arg}(G(j\omega))$ as a function of frequency ω (Johan et al., 2021).

Consider the dynamics of the closed-loop system deduced from Eq. (55) as:

$$\begin{cases} \dot{x}_m = A_m x(t) + B_m u(t) \\ y(t) = C_m x(t) + D_m u(t) \end{cases} \quad (55)$$

The associated transfer function is obtained by the ratio of output and input gains and is deduced from Eq. (56) as follows:

$$G(s) = \frac{Y(s)}{U(s)} = C_m (sI - A_m)^{-1} B_m + D_m U(s) \quad (56)$$

With $A_m = A - BK, B_m = BK_r, C_m = C, D_m = 0$

For robust stability analysis, we are particularly interested in infinite gain presented in Eq. (57) as follows:

$$|T(j\omega)| = \left\| \frac{PC}{1 + PC} \right\|_\infty \quad (57)$$

Where P represents the nominal system and C the controller. This maximum gain, plotted in the Bode diagram, is a key indicator for assessing the system robustness to uncertainties and guaranteeing closed-loop stability under non-ideal conditions.

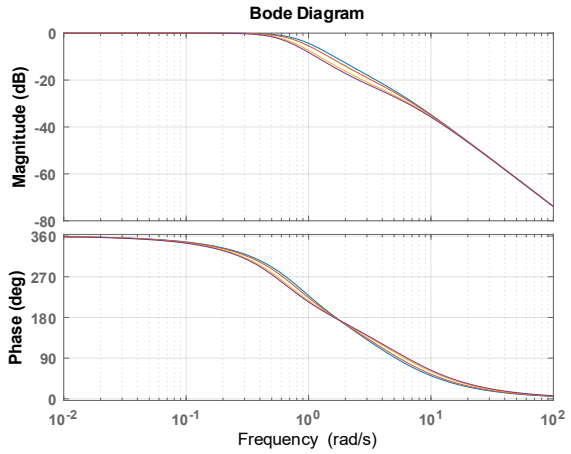

Figure 17: Bode Plot of cart position with mass uncertainty

The Bode diagram shows robust low-pass behavior of the carriage at different masses. At low frequencies ($0.01 - 0.2$ rad/s), the gain is unity with a constant phase shift, indicating that the system faithfully follows the setpoint with a slight delay. Above 0.2 rad/s, the progressive attenuation of gain and increase in phase shift show that the system is effectively filtering high frequencies. Curves superimposed on parametric variations, confirming the system intrinsic stability in the face of mass changes.

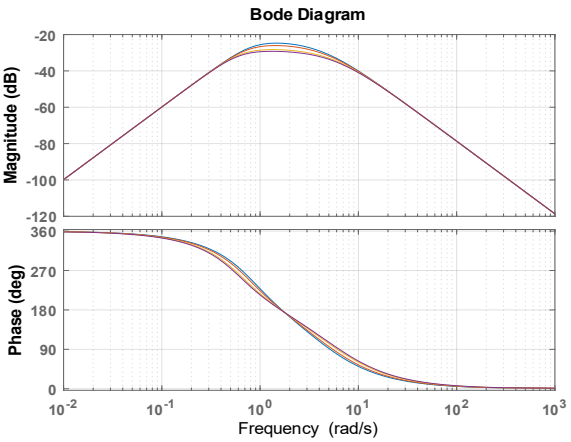

Figure 18: Bode Plot of pendulum position with mass uncertainty

The Bode diagram shows a typical bandpass behavior of the pendulum, with a resonance peak at 1 rad/s and a phase gradually evolving from 0° to 180°, marked by a phase shift of -90° at resonance. This frequency response reveals three distinct regimes: rigid at low frequency (constant gain, phase $\sim 0^\circ$), oscillating at resonance (maximum amplification, phase -90°), and flexible at high frequency (attenuation, phase -180°). Consistency between magnitude and phase confirms the system dynamic sensitivity around its natural frequency, necessitating avoidance of excitations at 1 rad/s to prevent excessive oscillations, while guaranteeing stable behavior outside this critical band.

The Bode diagram of the system response shows no hump, which is proof of the reduction of the H_∞ norm of T. We have thus demonstrated, as can be seen from Figs 17 and 18, that even for small uncertainties in the vicinity of the resonant frequency, the condition $\|T_\infty\| < 1$ is not violated, so we can conclude on the minimization of infinite gain.

6.2 Robust control by LQR synthesis

LQR synthesis is based on the minimization of a performance criterion deduced from Eq. (58) as follows:

$$J = \int_0^\infty (x^T Q x + u^T R u) dt \quad (58)$$

Where $Q \geq 0$ and $R > 0$ are weighting matrices translating state penalties and control efforts respectively. The objective is to determine the optimal state return of the form of the Eq. (59) below:

$$u(t) = -Kx(t) + K_r r \quad (59)$$

Where K is the optimal gain obtained by solving the algebraic Riccati equation.

For a linear, time-invariant system, this approach guarantees asymptotic stability of the origin, under the usual assumptions of controllability and absence of uncertainty. However, in real physical systems, uncertainties about intrinsic parameters (mass, stiffness, etc....) can alter closed loop behavior. A control is said to be robust if it preserves the stability and acceptable performance of the system despite these variations. In this article, the LQR control will exhibit local intrinsic robustness, particularly if the Q and R matrices are carefully chosen. Indeed, by widening the stability zone through stricter weighting of uncertainty-sensitive states, state feedback can compensate for the effects of moderate parametric disturbances. This phenomenon is illustrated by the figures, in which the system response to a step remains damped and converges to a steady state, despite simultaneous strong variations in parameter m. From an analytical point of view, this property can be linked to robust stability in the Lyapunov sense: if for any admissible variation ΔA, around the nominal model A, there exists a nominal parameter $P > 0$ such that we have Eq. (60) below:

$$A_\Delta^T P + P A_\Delta < 0 \quad (60)$$

with $A_\Delta = A - BK$

In order to evaluate the robustness of the controller against variations in user mass, a step

response analysis is performed. Figures 19 and 20 illustrate the impact of mass uncertainty on Segway control dynamics.

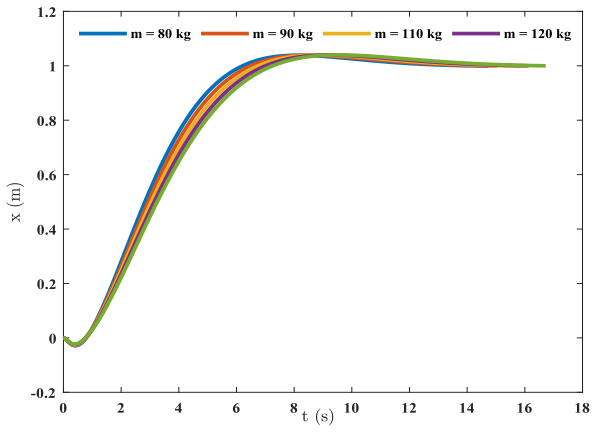

Figure 19: Response to a cart step with mass uncertainty

The response of the cart to a step input is shown in Figure 19. It remains stable and converges to the same final position for mass uncertainty, with minimal variations in dynamic characteristics such as overshoot and response time. This invariance of performance in the face of mass variations highlights the robustness of the state feedback control law with respect to this parametric uncertainty.

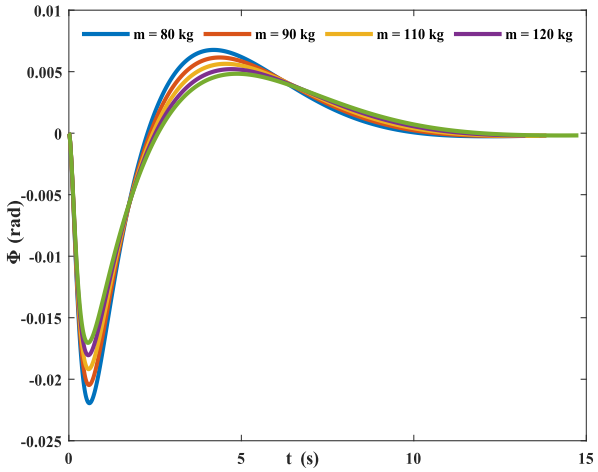

Figure 20: Response to a pendulum step with mass uncertainty

The pendulum response to a step input is shown in Figure 20. It shows rapid convergence to zero for all mass values, with small transient oscillations. The amplitude and duration of these oscillations remain moderate despite the mass uncertainty, reflecting good damping capability.

This uniform stability confirms the robustness of state feedback control in the face of system mass variations. Many studies have highlighted this property of resilience to moderate parametric variations, in particular when the uncertainties are additive or multiplicative and the dynamics of the system remains dominated by its main modes (Kwakernaak et al., 1972; Khalil et al.,1996).

7. Conclusion And Future Directions

In this paper, we proposed a rigorous approach to uncertainty management and state estimation for a Segway type personal transporter, combining a Kalman observer with a robust adaptive control strategy. The aim was to maintain system stability and performance despite significant variations in the user mass around $\pm\Delta m$. The results obtained show for the first time that the observer, in the absence of noise and disturbances, enables efficient reconstruction of the system state with negligible error. Furthermore, the MRAC type control demonstrated excellent adaptability in the face of parametric uncertainties, guaranteeing stable, high performance robot behavior. This synergy between state estimation and real-time adaptation is an essential lever for the development of intelligent mobility platforms capable of adjusting to users and the environment. Our future work will explore the integration of neural networks to improve online identification of unmodeled dynamics, or the extension of this approach to multi-user scenarios and rough terrain, could further enhance the autonomy and robustness of these systems.

Funding Information

There is no funding for this paper

Author Contributions

- **Arold's Elian KANKEU KENNE:** Conceptualization, Methodology, Modeling, Writing Original Draft, Theorem, Simulation, Investigations, Software.
- **Pascal KAMENI:** Literature Review, Modeling, Simulation, Optimization Algorithms, Writing Review and Editing, Software.
- **Ibrar Ahmad:** Literature Review, Writing Review and Editing, Simulation, Software.
- **Maxim Idriss MELI TAMETANG:** Methodology, Software Implementation, Resources, Supervision, Simulation, Software.
- **David YEMELE:** Methodology, Conceptualization, Critical Review, Proofreading, Supervision, Visualization, Project Administration, Simulation, Investigations.

Declaration Of Competing Interest

The authors declare that they have no known competing financial interests or personal relationships that could have appeared to influence the work reported in this paper.

Acknowledgements

The authors are grateful to the anonymous reviewers and editor for their insightful comments, which helped improve the content of this paper.

References

Astrom, K.J. 1989. Bjorn Wittenmark. In Adaptive Control. Addison Wesley.

Astrom, K.J., and Wittenmark, B. 2008. Adaptive control, Dover publications. INC. Mineola, New York.

Babazadeh, R., Khiabani, A. G., Azmi, H. 2016. Optimal control of Segway personal transporter. In 2016 4th International Conference on Control, Instrumentation, and Automation (ICCIA) (pp. 18-22). IEEE.

Cardozo, G.S.S., and Vera, L.M.S. 2012. Prototype for a self-balanced personal transporter. In 2012 Workshop on Engineering Applications (pp. 1-6). IEEE.

Castro, A., Adams, C., and Singhose, W. 2013. Dynamic response characteristics of a two-wheeled inverted-pendulum transporter. In 52nd IEEE conference on decision and control (pp. 1532-1537). IEEE

Chantarachit, S. 2019. Development and control Segway by LQR adjustable gain. In 2019 International Conference on Information and Communications Technology (ICOIACT) (pp. 649-653). IEEE.

Choi, D., and Oh, J.H. 2008. Human-friendly motion control of a wheeled inverted pendulum by reduced-order disturbance observer. In 2008 IEEE International Conference on Robotics and Automation (pp. 2521-2526). IEEE.

Grasser, F., D'arrigo, A., Colombi, S., and Rufer, A.C. 2002. JOE: a mobile, inverted pendulum. IEEE Transactions on industrial electronics, 49(1), 107-114

Hespanha, J. P. 2007. LQG/LQR controller design. Undergraduate Lecture Notes, University of California, Santa Barbara, California, USA.

Hughes, B.G. 2009. The Unique Physics of the Segway PT Balanced at All Times. American Journal of Physical Medicine & Rehabilitation, 88(1).

Johan, Å. K., Murray Richard, M. 2021. Feedback systems: an introduction for scientists and engineers. Princeton university press.

Kamen, D.L., Ambrogi, R.R., and Heinzmann, R.K. 1999. U.S. Patent No. 5,975,225. Washington, DC: U.S. Patent and Trademark Office.

Khalil, I.S., Doyle, J.C., Glover, K. 1996. Robust and optimal control (Vol. 2). New York: Prentice hall.

Kwakernaak, H., Sivan, R. 1972. Linear optimal control systems (Vol. 1, p. 608). New York: Wiley-interscience.

Landau, Y. D., and Dugard, L. 1986. Commande adaptative : aspects pratiques et théoriques. (No Title).

Morrell, J. B., and Field, D. 2007. Design of a closed loop controller for a two wheeled balancing transporter. In 2007 IEEE/RSJ International Conference on Intelligent Robots and Systems (pp. 4059-4064). IEEE.

Narendra, K.S., and Annaswamy, A.M. 2012. Stable adaptive systems. Courier Corporation.

Navinkumar, T.M., Praveen, A.A.A., Sasirekha, P., Gokila, P.V., and Kalaivani, C. 2022. Design of DC-DC Converter based Self Balancing Segway Transporter for Indoor Applications. In 2022 6th International

Conference on Computing Methodologies and Communication (ICCMC) (pp. 23-26). IEEE.

Ogata, K. 2010. Modern Control Engineering (5th ed.). Prentice Hall.

Pawar, R.J., and Parvat, B.J. 2015. Design and implementation of MRAC and modified MRAC technique for inverted pendulum. In 2015 International Conference on Pervasive Computing (ICPC) (pp. 1-6). IEEE.

Pilon, J. 2019. Commande adaptative robuste par modèle de référence d'un quadricoptère. Ecole Polytechnique, Montreal (Canada).

Sharma, M., Sharma, R., Singh, K., Sinha, V., Tadavi, S., Sharma, M., Tadavi, S. 2015. Segway–the human transporter. IJIRST–International Journal for Innovative Research in Science & Technology, 1(1), 128-132.

Skogestad, S., Postlethwaite, I. 2005. Multivariable feedback control: analysis and design. john Wiley & sons.

Tao, G., 2003. Adaptive control design and analysis. John Wiley & Sons.

Wong, S. M. 2010. Robotic Riding Mechanism for Segway Personal Transporter (Doctoral dissertation, Chinese University of Hong Kong).

Yin, C.Q., Li, L., Lv, A.Q., and Qu, L. 2007. Color image watermarking algorithm based on DWT-SVD. In 2007 IEEE international conference on automation and logistics (pp. 2607-2611). IEEE.

Cite the Article: Arold's Elian Kankeu Kenne, Pascal Kameni, Ibrar Ahmad, Maxim Idriss Meli Tametang, David Yemele (2026). Adaptive and Robust Control For Uncertainty Management in Autonomous Vehicles : The Case Of The Segway. Information Management and Computer Science, 9(1): 01-11.